Utrecht University

Bachelor thesis - June 2016

Optical characterisation of PbSe and CdSe 2D superstructures

Gerben van der Werf

supervised by

Maryam Alimoradi Jazi MSc. (CMI)

Abstract

Self-assembled nanocrystal solids show promising results as an active layer in optoelectronic devices. Atomically coherent 2D square superstructures are prepared by oriented attachment of truncated nano cubes of PbSe in which the quantum dots are connected by their {100}-facets. The optical absorption properties of these 2D superstructures are investigated by Fourier transform infrared spectroscopy. The absorption measured from several samples is found to be $1.5 \pm 0.4\%$. Furthermore, a new setup is built up to investigate the absorption and luminescence of the superstructures at room and low temperature.

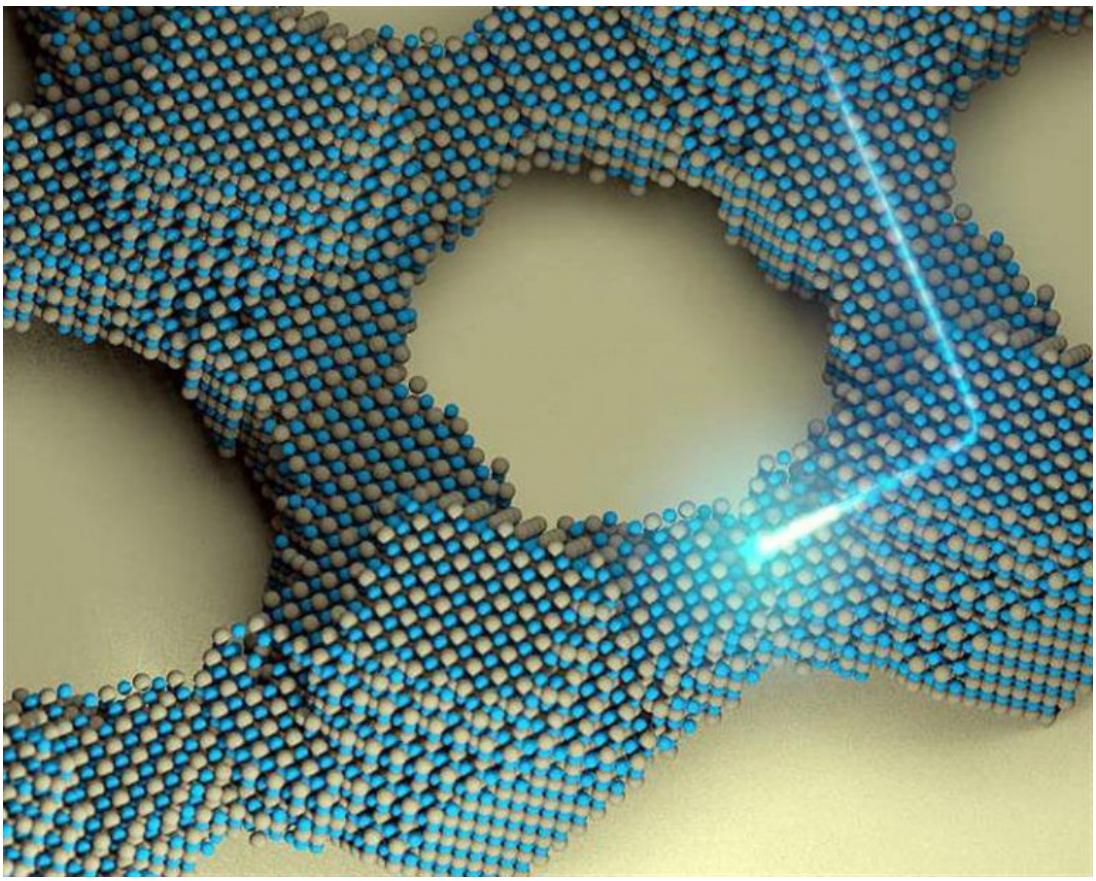

Contents

Introduction

Searching for new and interesting materials, nanoparticles really are a hot topic. Those nanoparticles have interesting properties that are mainly present because of their small size. A quantum dot is a special nanocrystal, namely a nanoparticle that is confined in all three spatial directions.

Fundamental and applied sciences are interested in these quantum dots. From the latter perspective, quantum dots are likely to be on of *the* new materials in all kind of applications, among them next-generation light detectors, emitting diodes (LED's) and even solar cells. From the fundamental perspective, the small nanoparticles might even be more interesting because they open up a complete new field of research.

This bachelor thesis is only one small link in the entire chain of applied and fundamental research. 2D superstructures of oriented attached PbSe and CdSe are investigated with optical experiments. Those 2D superstructures have remarkable properties. From a well-known 2D material, graphene, is reported that it absorbs light quanta per monolayer[1]. It is unknown if the 2D superstructures of PbSe and CdSe also have this property. This brings us to the first research question: Does a PbSe 2D superstructure with a square geometry also absorb a light quantum of the theoretically predicted value of 2.3% per monolayer?

The second part of this bachelor thesis is dedicated to the design of a new fluorescence microscope setup. The goal is to study the luminescent properties of the materials mentioned, mainly 2D CdSe superstructures, with this setup. These properties can provide interesting information of the studied material.

This thesis is divided in several sections, starting out with an introduction to the theory. This section is followed by subsequently the experimental part, the results, discussion, conclusion and the outlook. These parts summarise what work has been done, what work has to be done and what is discussed about the work done in the past months. And, as a closing section, the acknowledgements.

Source picture on the front page:
`http://techmezine.com/latest-electronics-products-news/quantum-dot-work-to-bring-new-era-for-electronics/`

1 Theory

1.1 Quantum Dots

Quantum Dots are nanocrystal semiconductors which are confined in all three spatial directions. [2] Especially within the range from 1 to 10 nm, the particle properties differ from bulk material which makes them interesting particles to study, both in fundamental and applied research. This differing properties are mainly caused by two effects: a large surface to volume ratio and quantum confinement of the exciton Bohr radius. The exciton Bohr radius depends on the effective masses of the electron and the hole and can be calculated with

$$a_0 = \frac{\hbar^2 \epsilon}{e^2} \left(\frac{1}{m_e^*} + \frac{1}{m_h^*} \right). \tag{1}$$

There are two major ways of thinking about the striking optical properties of quantum dots: a top-down approach and a bottom-up approach[3].

Top-down The top-down approach makes use of two equations:

$$E_g^{tot}(D) = E_g^0 + E_{n,l}^{conf}(D) = E_g^0 + \frac{2\hbar^2 \chi_{nl}^2}{m_e^* D^2} + \frac{2\hbar^2 \chi_{nl}^2}{m_h^* D^2} \tag{2}$$

$$E_g(r) = E_g^0 + \frac{\hbar^2 \pi^2}{2r^2} \left(\frac{1}{m_e^*} + \frac{1}{m_h^*} \right) - J_{e-h} + E_e^{pol} + E_h^{pol} - 0.248 E_{Ry}^*. \tag{3}$$

In Eq.2 the confinement energy is added to the normal band gap energy as a function of the diameter D. It is clear that with decreasing size (D) the energy of the bandgap becomes larger. Important to note is that this equation only holds in the strong-confinement regime. Basically, that is the regime where the radius of the particle r is still much smaller than the exciton Bohr radius a_0 and it means that the kinetic energy of the electrons and holes is much larger than the Coulombic interaction between those particles. In Eq.3 the Coulomb force is considered (J_{e-h}) and combined with Eq. 2 this equation accounts for the discretisation of the energy levels at the band-edges. Of course, this equation holds then for the weak-confinement regime. These two effects can be visualised as in Fig.1a. It is clearly visible that with decreasing size the bandgap increases and that with decreasing size the discrete levels are more and more distinct[3].

Bottom-up In the bottom-up approach, the nanocrystal is considered to be composed of atoms, all with an individual atomic orbital (AO). When there is more than one particle, molecular orbitals (MOs) are formed, in a higher energy anti-bonding MO and a lower energy bonding MO. In the case of two particles, there are only two interesting levels, the lowest unoccupied state (LUMO) and the highest occupied state (HOMO). With increasing number of particles the number of MOs grows as well. This leads to more energy levels and therefore the gap between HOMO and LUMO decreases. Because the intermediate energy states are more probable, the density of the MOs is higher at intermediate energy and lower at the energy extremes. In the bulk limit, there is a so-called band gap, which is the gap between HOMO and LUMO and the distinct energy levels are no longer visible. Intermediate between the molecule and the bulk crystal is the nanocrystal, having discrete conduction and valance levels. The band gap between conduction and valence band is larger than the bulk crystal band gap and smaller than the HOMO-LUMO gap of the single molecule. This regime accounts for the fact that the band gap energy is size-dependent, higher than the bulk band gap and that discrete energy levels are visible: Fig. 1b.

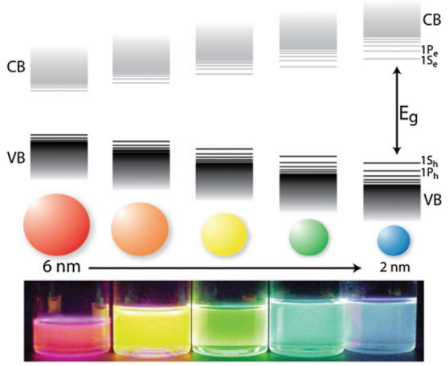

(a) Top-down approach towards nanoparticles. Decreasing size causes an increase in band gap and discrete states near the band edges[3].

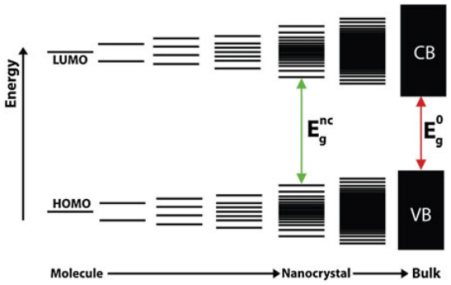

(b) Bottom-up approach towards nanoparticles. With an increasing amount of atoms per quantum dot the band gap energy decreases and the density of states increases from one discrete state to the bulk limit with bands[3].

Figure 1: Quantum dots, Top-down vs. bottom-up approach

PbSe is chosen as one of the materials to work with because it has several nice properties. It has a small direct bandgap in the NIR region and can absorb light efficiently. Furthermore, it has a large Bohr radius and thus strong quantum confinement effects for particles of approximately 5 nm. The ability of tuning the bandgap by changing the particle size is of particular interest in 2D honeycomb structures, that contain Dirac cones in their band structure but also have this tuneable bandgap, whereas graphene lacks this property[4]. The material is already in use as active material in emitting diodes, lasers and IR-detectors. For the use in next-generation quantum dot-based solar cells, this material might be a very useful in application because of its ability to absorb efficiently in NIR-region. As depicted in Fig. 2, half of the energy of the solar energy is in the NIR-region[5].

Furthermore, the quantum dots of interest can be seen as truncated cubes which make them suitable for oriented attachment, which we will discuss in a minute. The truncation is dependent on the size of the quantum dots. In Fig. 3 a cube truncation model is shown. Another model is the octahedral model but we will not consider this because it is out of the scope of this bachelor thesis[6].
For both practical purposes and fundamental interest it is convenient to have CdSe structures as well as PbSe. The method of cation exchange (will be discussed later 2.2) is a quite simple method to convert the PbSe crystal lattice into a CdSe lattice, preserving its nano geometry and crystallinity. CdSe has a band gap in the visible range[6] .

From a more fundamental perspective, the honeycomb lattices of CdSe and PbSe are predicted to have a rich and interesting band structure, in both the conduction and the valence band. A recent theoretical study has shed light on these structures: for example the valence band of the silicene-type lattice of CdSe has a gap at the Dirac points which can be tuned by applying an electric potential. Furthermore, the graphene-type lattice has the remarkable property of being a topological insulator when a strong spin-orbit coupling is combined with the honeycomb geometry. Previously, this was also predicted for graphene but this material doesn't have a spin-orbit coupling that is strong enough. To check these theoretical predictions, it would be very interesting to experimentally create these honeycomb lattices[4].

1.2 Oriented Attachment

Oriented attachment is the atomic coupling of colloidal nanocrystals in a crystal structure with a high level of ordering and one of the methods to make the above described honeycomb

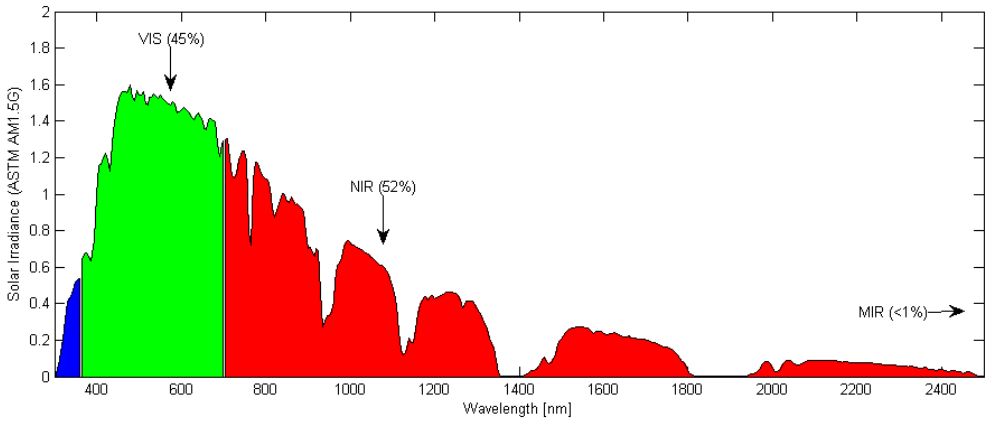

Figure 2: Solar spectrum [7]

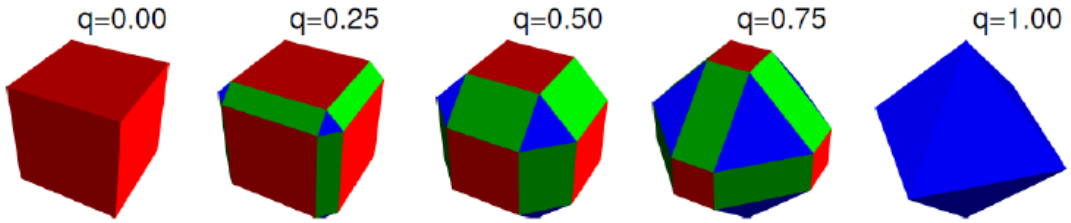

Figure 3: Red: {100}, Green: {110} Blue: {111}, q is the truncation level. [6]

structures. The process of oriented attachment is governed by certain driving forces, but there is still debate about the nature of oriented attachment. In Table 1, a summary of the forces that are considered in the process is given [8] [9].

However, the best candidate for the driving force of the attachment of PbSe is likely to be the surface energy reduction because the crystal growth is highly facet-specific. Because the PbSe particles have well-defined facets, they can take part in the oriented attachment process. The different facets of the truncated PbSe have different energies. The facets to be considered are {100}, {110} and {111} as is depicted in Fig.3. The facet with the lowest energy is the {100}-facet, followed by {110} and then {111}[6]. With thermodynamic arguments, three theories can be proposed for the nature of the facet-specificity of the attachment:

- Facet with highest surface energy difference is likely to attach
- Facet with highest surface energy is likely to attach
- Facet with lowest surface energy is likely to attach

Interaction	**Attractive/repulsive**	**Origin**
Sterical hindrance	Repulsive	Ligands
Electrostatic interactions	Repulsive/attractive	ionic nature of particles
Surface energy reduction	Attractive	Dangling bonds on surface
Dipole moment	Attractive	Separated electric charges in system
Van der Waals interactions	Attractive	Permanent/induced dipoles

Table 1

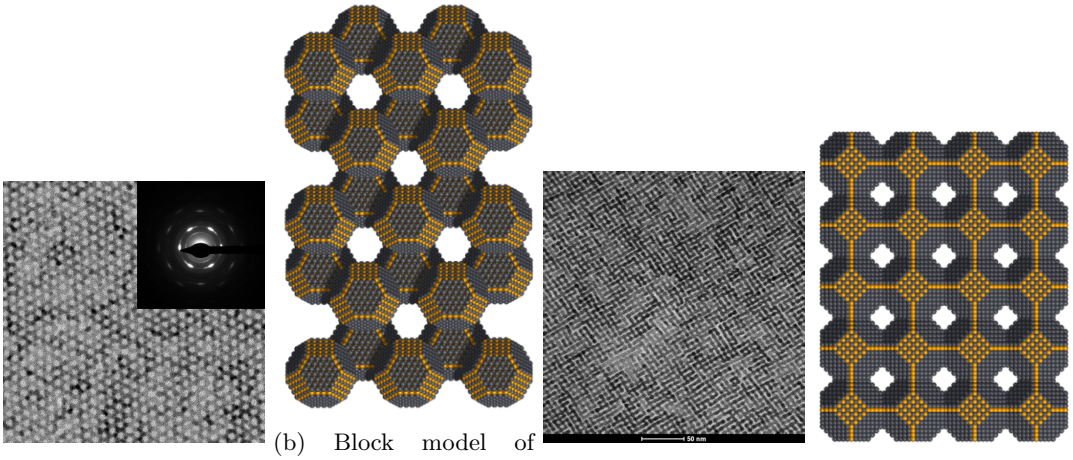

(a) TEM picture of honeycomb lattice, inset electron diffraction data

(b) Block model of honeycomb structure, {111}-facet is pointing upward

(c) TEM picture of square lattice, inset electron diffraction data

(d) Block model of square structure, {100}-facet is pointing upward

Figure 4: Models for honeycomb and square lattice, accompanied with TEM and electron diffraction data

The first theory can be argued with help of thermodynamic arguments, neglecting entropic terms:

$$\Delta E\left(OA\right) = E\left(attached\right) - E\left(initial\right). \tag{4}$$

The second theory states that the most unstable facet will reduce its energy and according to the third theory, the most stable facet will attach[9][8]. This can be understood by incorporating the effect of ligands. Ligands stabilise the nanocrystals in dispersion and the surface lowest in energy needs the least ligands in order to be stable. Because the ligands are less strongly attached (or less ligands are attached) to the low energy facet, they have a so-called higher adsorption-desorption rate and therefore this facet is more likely to be free to take part in an attachment process[6]. Recent research showed the correctness of the third theory in the case of PbSe quantum dots. Attachment occurs via the {100}-facets by {100}- and {111}-facets facing upwards in square and honeycomb geometries (Fig. 4), respectively. The striking property of being single crystalline is caused by the facet-specific attachment. Even stronger, the quantum dots are found to be rotating until they are in the right crystal plane alignment, enhancing a highly ordered system[10].

It is important to distinguish oriented attachment from another process which is called self-assembly. In the latter, van der Waals forces and sometimes entropic factors are the key to understanding the mechanism, whereas in the former, it is most likely that e.g. Coulombic interactions, dipolar forces and surface energy reduction are the driving forces[6], [11]. The second difference is the nature of the bonding between the two processes: in oriented attachment the bonding is irreversible and in self-assembly it is a free energy governed equilibrium. Self-assembly is driven by the van der Waals interactions between capping ligands and the higher entropy caused by the increased free space per particles due to the ordering[12]. Oriented attachment is, as stated above, irreversible. This is because the crystal facets of the nanocrystals (or quantum dots) are attached via atomic interactions[6].

1.3 Absorption

Absorption is a well-known process whereby a photon is absorbed, causing an electron (or another particle) to go into an excited state. An absorption spectrum can be made by exposing a sample to light from a certain light source and to compare the incident amount of light with the amount of light after interaction with the sample, Fig. 5a. We know from the Lambert-Beer law that the thickness and concentration of a sample also influences the amount of absorbed light:

$$E = \epsilon c d, \tag{5}$$

where E is the extinction, ϵ the extinction coefficient, c the concentration of the sample and d the thickness. Of course this is nicely applicable for a liquid sample. However, recent theoretical and experimental work shows that monolayers of graphene also absorb a significant fraction of light when exposed to it (2.3%). This value is actually a quantised value which is a multiple of the amount of monolayers the system has, as long as the material is a 2D system[1].

It is important to know where this value of 2.3% comes from. In the following lines, a calculation is shown that results in a value of π multiplied by the fine structure constant α, which has the value of approximately 1/137. Apparently, the absorption quantum is solely defined by physical constants. Consider a monolayer of graphene exposed to some incident light perpendicular to it with an electric field $\vec{\Theta}$ and frequency ω. Then, the incident light flux is given by the following expression:

$$W_i = \frac{c}{4\pi}|\vec{\Theta}|^2. \tag{6}$$

The amount of light of this incident flux can be calculated by means of Fermi's golden rule, making use of a perturbed Hamiltonian and the coupling between initial and final states. The amount of light that is absorbed is equal to

$$W_a = \eta\hbar\omega, \tag{7}$$

where η is equal to the number of absorption events and can be calculated with Fermi's golden rule 8, $\hbar\omega$ is the energy that an electron gets when it absorbs a photon.

$$T_{i\to f} = \frac{2\pi}{\hbar}|\langle f|H'|i\rangle|^2\rho. \tag{8}$$

We can use this expression to calculate the number of absorption events η:

$$\eta = \frac{2\pi}{\hbar}|M^2|D, \tag{9}$$

where M contains the matrix elements of the perturbed Hamiltonian with the final and initial states and D is the density of states at the energy level of interest, which is in the case of graphene equal to:

$$D\left(\hbar\omega/2\right) = \frac{\hbar\omega}{\pi\hbar^2 v_F^2}. \tag{10}$$

This is the density of states for $2D$ Dirac fermions, which is linear in ϵ. The density is considered at energy $\hbar\omega/2$ because of momentum conservation. Next, the Hamiltonian that we use has to be a perturbed Hamiltonian and this one is proposed, for the case of the interaction of Dirac fermions with light:

$$\hat{H} = v_F\vec{\sigma}\vec{p} = v_F\vec{\sigma}\left(\hat{p} - \frac{e}{c}\hat{A}\right) = \hat{H}_0 + \hat{H_{int}}, \tag{11}$$

where H_0 and H_{int} are the normal and interaction Hamiltonians respectively, v_F is the Fermi velocity, $\vec{\sigma}$ are the Pauli matrices, $\hat{p}$ is the momentum and $\hat{A}$ is some potential which in our case is equal to

$$\hat{A} = \frac{ic}{\omega}\vec{\Theta}. \tag{12}$$

We can make use of this Hamiltonian and put it into Fermi's golden rule 8:

$$|M|^2 = |\langle f|v_F\vec{\sigma}\frac{e}{i\omega}\vec{\Theta}|i\rangle|^2. \tag{13}$$

This can be calculated and the result yields a nice expression for coupling between final and initial states:

$$|M|^2 = \frac{1}{8}e^2v_F^2\frac{\Theta^2}{\omega^2}. \tag{14}$$

We can use this found value and calculate W_a:

$$W_a = \eta\hbar\omega = \frac{2\pi}{\hbar}|M|^2D\hbar\omega = \frac{2\pi}{\hbar}\frac{1}{8}e^2v_F^2\frac{\Theta^2}{\omega^2}\frac{\hbar\omega}{\pi\hbar^2v_F^2}\hbar\omega = \frac{1}{4}\frac{e^2\Theta^2}{\hbar}. \tag{15}$$

To finish is completely, we only have to divide W_a by W_i:

$$\frac{W_a}{W_i} = \frac{\frac{e^2\Theta^2}{4\hbar}}{\frac{c}{4\pi}|\vec{\Theta}|^2} = \frac{\pi e^2}{\hbar c} = \pi\alpha \approx 2.3\%. \tag{16}$$

The reason postulated for this quantised absorption is that the material is two-dimensional and has a gapless electronic spectrum[1].

Interesting enough, this quantised absorption per monolayer is found in graphene. There is only little deviation from this value of 2.3% when going to higher energies. When extra layers are added, the absorption quantum is clearly visible, per monolayer added, an extra 2.3% of the incident light is absorbed. Apparently, the theory predicted the experiment well. Important is that the reflectivity of graphene appears to be really low and can be neglected for practical purposes[1]. Even more interesting, the absorption quantum is also found in another material, namely a 2D InAs nano membrane, a semiconductor with a direct band gap[13]. This is interesting, particularly because of the band gap the material has: apparently the quantised absorption is not affected by the gap in the electronic spectrum and is only present because of the two-dimensional nature. For InAs also more layers are added to the monolayer and as long as the material thickness is smaller than the exciton Bohr radius, integer steps in absorption are found per added monolayer. However, the absorption quantum for this material is not equal to 2.3%. A local field correction factor has to be applied, containing a correction for the refractive index of the substrate used.

$$A_Q = \frac{\pi\alpha}{n_c} = \pi\alpha\left(\frac{2}{1+n}\right)^2 \tag{17}$$

where n_c is the local field correction factor and n is the refractive index of the substrate used. A value of approximately 1.6% is found both theoretically and experimentally[13].

If this theory holds for all 2D materials, our 2D superstructures of PbSe and CdSe should also have this absorption quantum.

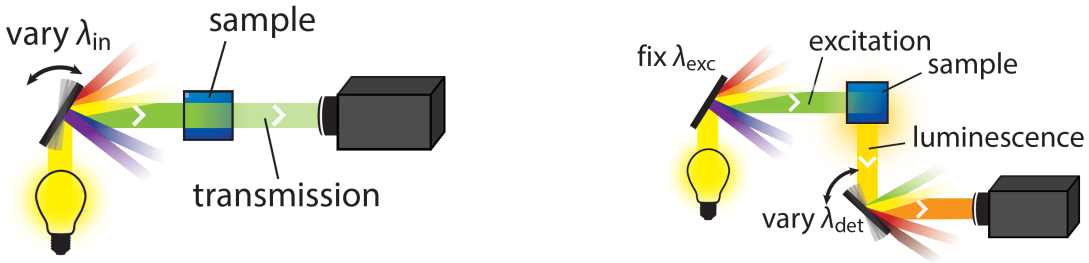

(a) Absorption

(b) Luminescence

Figure 5: Optical characterisation [14]

1.4 Photoluminescence

However, absorption is not the only interesting optical process. Or to put it even stronger, the interesting optical processes start after absorption. When an electron falls back to a lower lying energy state, or (in semiconductor physics) recombines with a hole, in a radiative manner this is called photoluminescence. In semiconductor physics this is the crossing of the band gap of an excited electron in the conduction band to the valence band and in literature this process is referred to as being an exciton (electron-hole pair) recombination. The prefix 'photo' is added because a photon is emitted in this process.

Photoluminescence is an easy method in the sense that the setup for an experiment is quite simple, yet it is as powerful as simple Fig. 5b. It is possible to obtain information about allowed optical transitions in a material and it gives insight in the relative rate of radiative and non-radiative decay or recombination. When photoluminescence is not present, non-radiative processes are taking over[15]. These processes are discussed in a second.

Photoluminescence happens especially at the surface, because the penetration depth of the incident light is about 1-10 μm in the case of a direct semiconductor, as for example PbSe and CdSe. This is an interesting feature because in this thesis the focus is mainly on 2D monolayer semiconductors, which is actually only a surface. This means that one dimension (the material thickness) of the crystal is smaller than the electron Bohr radius [13]. Photoluminescence, if present, would be really powerful for these 2D materials because it is sensitive towards discrete electronic states, which appear in our quantum dots. If the quantised absorption theory also holds for our material, around 1% of the incident light would be absorbed. This clearly limits the photo luminescent intensity because the more light is absorbed, the more light can be collected in case of photoluminescent behaviour. Just to have an impression of the material thickness that is used for this bachelor thesis, the quantum dots used are around 5 nm in size, the material thickness is therefore also around this size (and thus way smaller than 1μm). Important to recall, one of the parameters that control the photoluminescent intensity is the incident light intensity and the percentage of incident light that is absorbed. If the surface is full of defects, the luminescent behaviour is as a consequence severely suppressed by non-radiative recombination[15].

1.4.1 Non-radiative recombination

The energy of the incident light should always be at least the energy of the band gap and preferably higher. Thermalisation via phonon emission happens rapidly and the excited electrons relax to the lower lying states of the conduction band. The radiative recombination rate is usually slower than the thermalisation process and this is the reason that only the lower energy states are visible. Non-radiative decay reduces the radiative signal. There are two major types of non-radiative recombination: Shockley-Read-Hall recombination (SRH) and Auger recombination. It depends mainly on the major carrier density, i.e. electrons or holes,

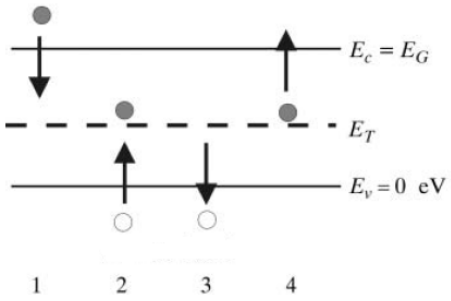

(a) SRH recombination, the different numbers represent different ways of phonon assisted recombination via mid-gap states

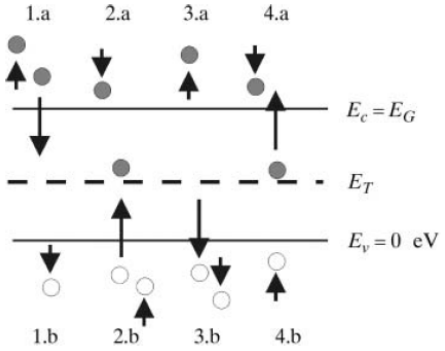

(b) Auger recombination, the different numbers represent different ways of recombination

Figure 6: Non-radiative recombination. Filled dots are electrons, circles are holes [16]

which recombination rate is dominant. The recombination rate is inversely proportional to the lifetime which we can equate as follows, assuming SRH recombination only to happen at two identical surfaces:

$$\frac{1}{\tau} = \frac{2S}{d} + \frac{B}{N}n + Cn^2, \tag{18}$$

Where τ is the carrier lifetime, S the interface recombination velocity, d the thickness of the optical active layer, N the average number of radiative recombination events required for a photon to escape the semiconductor, B and C parameters of the rates of radiative and Auger recombination respectively and n the carrier density. At low carrier density, the SRH recombination is dominant and no photoluminescence is observed. With increasing carrier density, the radiative recombination becomes more important while SRH events only contribute little to the total recombination. Only at higher carrier densities, Auger recombination is more important than both radiative and SRH recombination[15].

Shockley-Read-Hall recombination SRH recombination is a type of recombination that potentially is dominant in 2D semiconductors because of the low carrier densities. Discrete defects and impurities account for the SRH recombination, because recombination from these sites is energetically favourable. These impurities cause dangling bonds that create electronic mid-gap states that can act as a trap in the bandgap for an electron or a hole, Fig. 6a. The energy transfer is done by phonons of the crystal lattice[15].

Auger recombination Auger recombination is a process which is only dominant at high carrier density. This is because it involves three particles in the recombination process. Two electrons in the conduction band and one hole in the valence band are the particles in play, however, this whole process can be translated to the case of two holes and one electron[17]. One of the electrons is recombined with the hole giving its energy to the other electron which is then excited to a higher energy level, Fig. 6b.

Photoluminescence is a process that is temperature dependent Fig. 7. At lower temperatures more distinct peaks might be visible and the energy of the peak changes. The information that can be derived from the distinct peaks can be used to determine the origin of the photoluminescence, it can either be the normal near-band-edge emission or the emission from defects on the surface[18]. This feature can be used to determine the quality of the sample. However, having too many defects reduces the emission severely. With going to lower temperature, the thermalisation of the electrons to the lowest lying energy levels of the conduction band is very

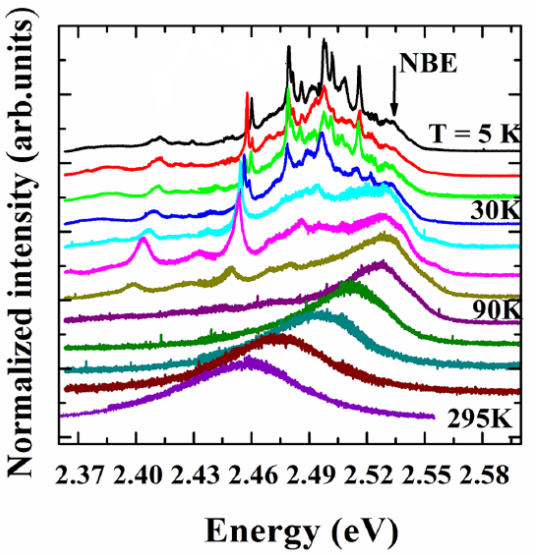

Figure 7: Example of temperature dependent photoluminescence in CdS nanowires[20]

rapid and only lower lying levels are visible, whereas at higher temperature higher lying levels can also contribute[17], [19].

To have the optimal photoluminescence efficiency, the surface should be in good condition. This might not be the case with all samples and a technique to enhance the surface condition is passivation. Passivation with a lead can enhance the photoluminescence intensity and prevents the quantum dots from oxidation[5].

2 Experimental

2.1 Oriented Attachment

The theory of the oriented attachment may not be completely developed yet, the idea of how to do oriented attachment in a lab is pretty easy. The oriented attachment of the PbSe QDs to form square superstructures is performed by using dispersions of QDs. Typically,350 µL of the suspensions is drop casted on top of an ethylene glycol substrate. The solvent of the dispersion (toluene) evaporates at the temperature of 20 °C, inducing self-assembly of nanocrystals and accompanying their oriented attachment via {100}-facets: Fig. 8. After heating to the temperature of 65-80 °C, well-developed connections between the nanocrystals with necks of 4.0 ± 0.2nm can be achieved. After attachment, the monolayer can virtually be transferred to any substrate, in this research a quartz glass is used to put the sample on. This transferring is done either by scooping the sample with the substrate or literally stamp the glass in a gentle way on the sample. TEM samples are collected by scooping the sample with a TEM grid. The experiment is carried out in a petri dish of 2.5 cm Ø[6] with different concentrations. The whole procedure is carried out in a nitrogen purged glovebox.

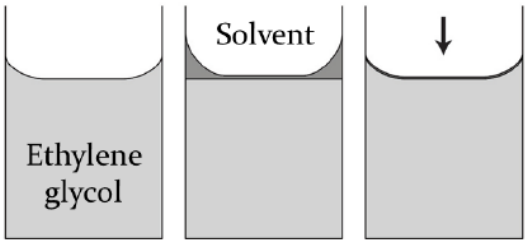

Figure 8: Oriented attachment procedure of quantum dots [9]

2.2 Cation Exchange

For practical purposes, it sometimes is convenient to have structures that absorb an emit in the visible spectrum instead of in the NIR region, like the PbSe QDs do with their small band gap. CdSe has a larger band gap and absorbs and emits in the visible region. Oriented attachment of CdSe quantum dots is impossible but it is possible to convert PbSe monolayers by cation exchange to CdSe structures. The main idea is that the Pb ions are replaced by Cd ions. The overall geometry (i.e. square or honeycomb) is not changed but the crystal structure changes from rock salt to zinc blende[6].

The procedure of cation exchange is not too difficult. The substrate with the sample on it is immersed in cadmium oleate, $C_{36}H_{66}CdO_4$, at a temperature of 120 °C for one hour. Then the sample is washed several times by methanol and toluene and dried in nitrogen atmosphere.

2.3 Experimental setup and techniques

2.3.1 Transmission Electron Microscopy

Transmission Electron Microscopy (TEM) is a Nobel Prize winning method or technique that makes use of an electron beam to expose the sample to, to make a high resolution image. The electron beam is focused on a sample and an image is made via an imaging device, Fig. 9. The method is actually an absorption technique, the difference is that electrons are used instead of photons. The use of electrons allows a exceptionally high resolution image, the atomic scale is visible. This high resolution is reached because electrons have a smaller de Broglie wavelength than light 19.

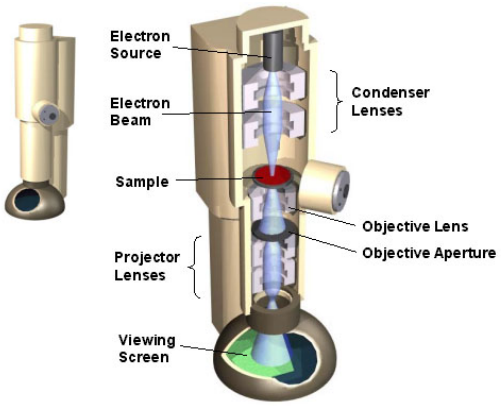

Figure 9: TEM setup [21]

$$\lambda = h/p \tag{19}$$

The electron beam is brought forth by an electron gun, a high voltage filament that produces electrons. These electrons are focused by lenses by means of electromagnetic interactions. By changing the magnetic power of the focusing lenses, the focus can be changed. The electron beam is focused in the right way to hit the sample in the most optimal way. After interaction with the sample, the electrons are collected in an image detector.

2.3.2 Fourier Transform InfraRed spectroscopy

Fourier Transform InfraRed spectroscopy is a technique used to obtain absorption, emission and reflectivity spectra of samples. The light source is coupled to a Michelson interferometer that gives a certain combination of wavelengths that can be adjusted by moving a movable mirror. Each combination of wavelengths is collected in an interferogram and converted to a normal spectrum of wavelength versus intensity via a Fourier Transform algorithm. The mechanism of this is far beyond the scope of this project, however it is good to mention that the signal to noise ratio of these devices is pretty good compared to normal absorption measurements. Furthermore, the FTIR device can be extended with a microscope, a very interesting feature, especially if you want to measure samples with a low coverage of the desired square monolayer, Fig.10a. It is also possible to add a reflectivity measurement with this device, the optical path is somewhat different then, compared to the optical path of the transmission experiment, Fig. 10b. With a rotatable mirror, the direction of the light can be changed and it can either be brought from the top side for transmission or from the down side for reflectivity measurements. The measurements with the Hyperion microscope are performed with 15 x 15 lenses and 200 scans with a resolution of $2\,\mathrm{cm}^{-1}$. Several measurements are performed with the normal FTIR, 40 scans are made per sample with a resolution of $2\,\mathrm{cm}^{-1}$ with an aperture setting of 1.5 mm. A quartz beam splitter is used with the Vertex 70 detector. The samples are put in a sample holder to protect them from the oxygen in air [22].

2.3.3 Fluorescence microscope

Charge Coupled Device A Charge Coupled Device (CCD) camera relies on the same principle as a silicon photodiode does. A photodiode makes use of a p-n junction, a combination of a positively doped (p-type) and a negative doped (n-type) semiconductor. The majority carriers

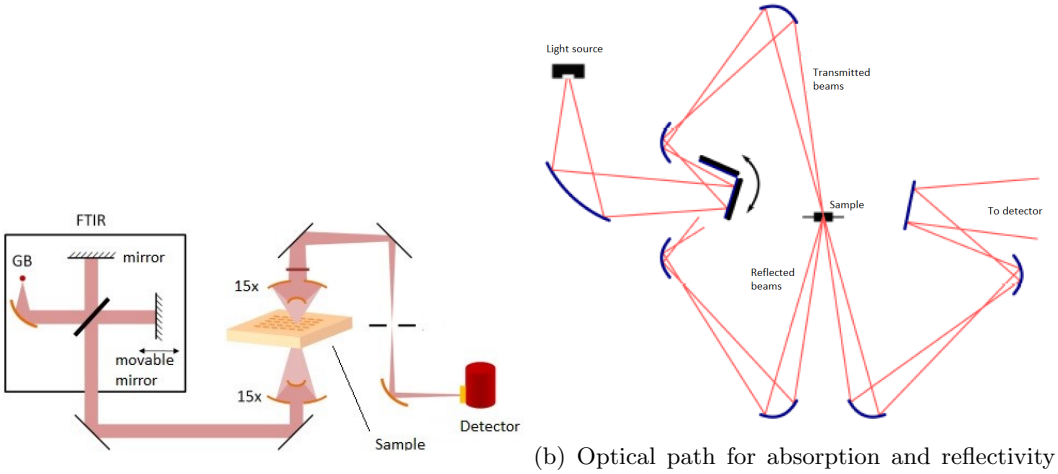

(a) Complete FTIR absorption setup[23]

(b) Optical path for absorption and reflectivity measurements[24]

Figure 10: FTIR setup

in p-type semiconductors are the holes whereas the majority carriers in n-type semiconductors are the electrons. Around the junction, which is the connection between the oppositely doped semiconductors, an equilibrium will be reached with two competing mechanisms that keep the electrons and holes 'in place'. First, the holes from the p-type material tend to migrate to the n-type material and the electrons from the n-type to the p-type material. Subsequently, a potential difference is formed and an electric field will be present because there is a charge difference between the materials. Because of this electric field, electrons and holes are no longer able to cross the potential and migrate to the other material. This is the equilibrium which can only be overcome by a external potential. A positive bias can be created to connect the positive side of a battery to the p-type material and the negative side to the n-type material. When the potential of the battery is high enough to overcome the formed electric field in the depletion region, the region around the p-n junction, a current is flowing. Now, when a photon excites an electron in the depletion region, a current will flow because of the electric field that causes the electrons and holes to flow to opposite direction. This current can be measured. [25] [26]

A CCD works with the same principle as the photodiode does, except that in a CCD an array of p-n junctions is used, also referred to as pixels. When photons hit the surface, electrons are collected in the depletion layer of the junction and then transferred to a read-out pixel that is converted to digital information in a computer. This transfer of electrons is done by a voltage pulse sequence that transfers the electrons from one potential well to another, successively in parallel and serial direction Fig. 11b. Important to note is that the detector can be saturated. If one pixel is illuminated with a very large number of photons, not all photons can excite an electron that will be collected in the read-out procedure.

Luminescence The setup of the fluorescent microscope is based on inverted microscope and is sketched in Fig. 13a. The sample can be illuminated with a tungsten-halogen light source, coupled to a monochromator to adjust desired excitation wavelength, via a beam splitter and an objective. The tungsten-halogen light source can be changed to a laser light source if higher light intensity is needed. The beam splitter is perfectly designed for excitation below 500 nm and emission between 500 and 800 nm (the transmission and reflection are showed in Fig. 13c). The sample is mounted in a cryostat to allow experiments at low temperature. The light that is reflected and scattered from the sample is collected via the same objective. With the rotatable mirror and a camera the sample can be visualised via a tube lens and with the movable stage of the cryostat the position of the sample can be adjusted to bring it in focus. When the sample

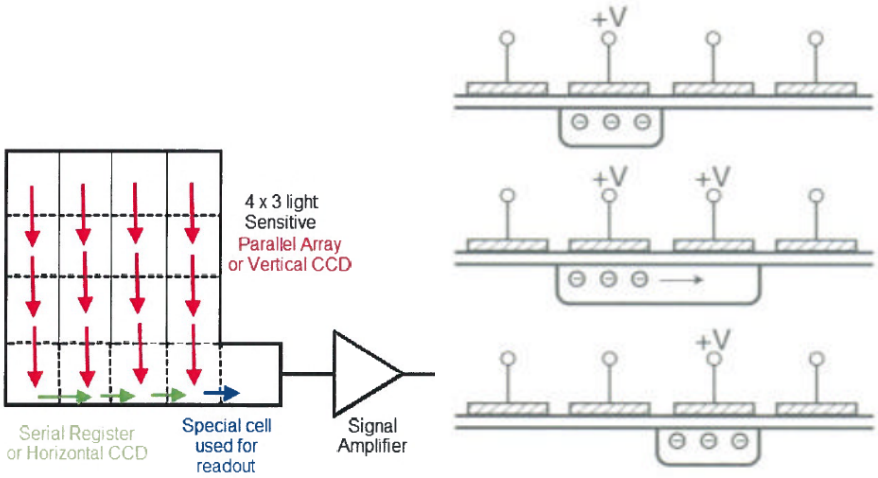

(a) Overview over the read-out procedure of an arry of pixels [26]

(b) A picture showing the migration of charge in a CCD-device [27]

Figure 12

is in focus the rotatable mirror can be brought down and the photoluminecent signal can be detected with the CCD detector.

Absorption With minor changes to the luminescence setup, transmittance can be measured as well, but the setup is then a normal microscope setup, Fig.13b. The same tungsten-halogen light source can be used and the monochromator doesn't play a role in this setup, which yields a white light spectrum. With the collimator on a different place the light can be brought from the back of the cryostat. The light is focused by means of a combination of two close-positioned lenses (convex lens). The light is again collected via an objective, a tube lens and finally the CCD detector.

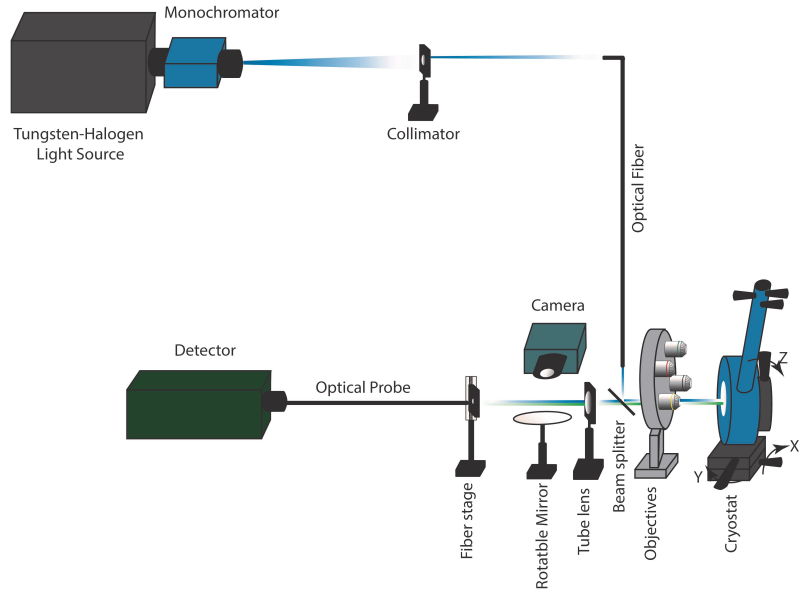

(a) Luminescence setup

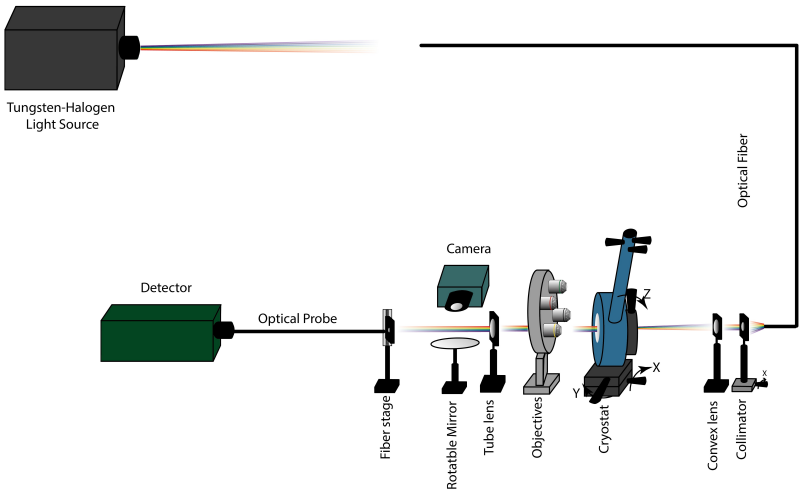

(b) Absorption setup

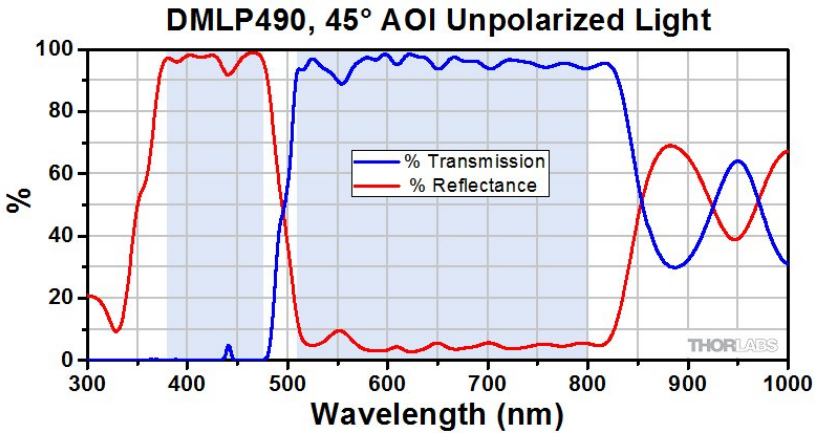

(c) Beam splitter transmission and reflectance in luminescence setup[28]

Figure 14

3 Results

3.1 FTIR

In this section, results from absorption measurements carried out with FTIR are analysed. On those measurements, calculations are performed to withdraw the absorption value at the exciton peak of the sample. The results of this calculation were quite interesting, however no well-defined quantised absorption value could be obtained yet. In addition, the method with the combination of microscope and FTIR device is fine-tuned. The samples presented in this section are all made in Delft. The samples are measured in different positions to account for the inhomogeneity of the samples.

The samples are measured in the units of absorbance which has to be turned into units of absorption by means of Eq. 20.

$$T = 10^{-A} \tag{20}$$

Where A is absorbance. We assume $R \approx 0$ and then it is possible to calculate the absorption, simply by subtracting T from 1:

$$1 - T = A, \tag{21}$$

where A is absorption.

Due to thermal effects, the baseline of the graphs is not always starting at zero intensity. This fact is counteracted by a correction.

After performing a correction for the quartz substrate on the absorption value of 2.3% found for graphene, a value of 1.5% for PbSe is obtained. This is found by using Eq. 17 and the value of the refractive index of quartz: 1.4584[29].

3.1.1 Sample 1

Sample 1 is made via oriented attachment with a solution of 15 µL QDs, synthesised by Joep Peters MSc., diluted in 1 mL toluene.

The TEM picture, Fig. 15, shows the large-scale square structure. However, the sample is not completely homogeneous. The FTIR data shows both the normal measured sample, Fig. 16a, as well as the sample measured with the microscope, Fig. 16b. Sample 1A does not so much exhibit the plateau shaped peaks but more the hill shaped peaks: this is a clue that the connection between the quantum dots might not be very strong. The peaks are clearly visible and the resolution acceptable. Sample 1B, measured under the microscope, has a lower resolution. There is a big difference in all the results which can be addressed to the fact that the sample is inhomogeneous. Accumulated quantum dots and empty spots on the substrate influence a measurement heavily, this is the main reason different sample positions are measured. The spots selected with the microscope had

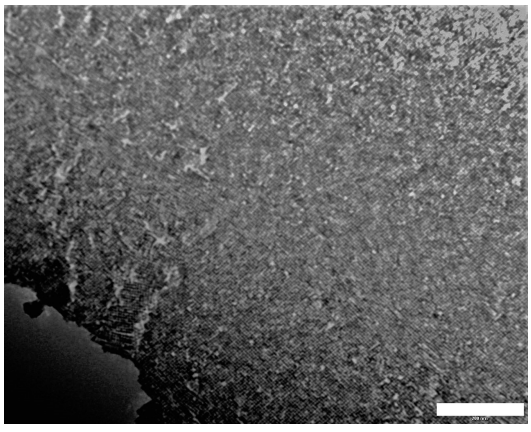

Figure 15: TEM of sample 1A and 1B, scale bar is 200 nm

almost the same value, this might be the case due to the fact that it is possible to select a nice homogeneous area of the sample by means of the microscope.

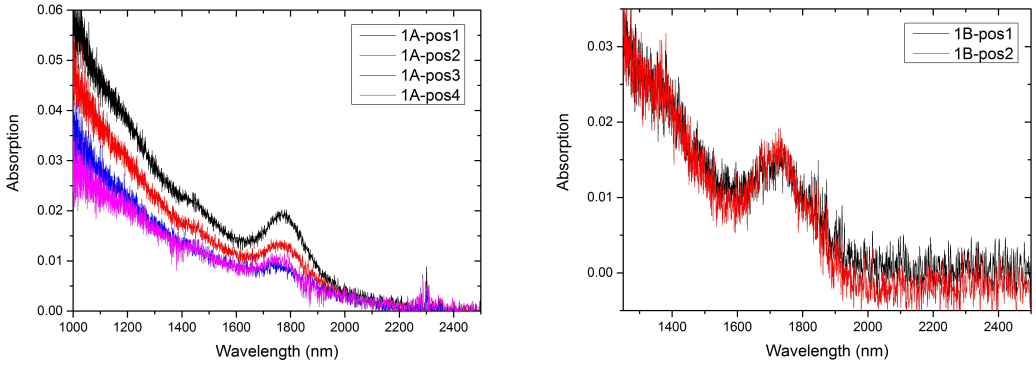

(a) Sample 1A

(b) Sample 1B

Figure 16: FTIR data

Sample	**Position**	**Absorption (%)**	**Wavelength (nm)**
1A	1	2.0	1767
	2	1.3	1767
	3	0.9	1767
	4	1.1	1767
1B	1	1.5	1728
	2	1.6	1739

Table 2: Absorption data of sample 1

One of the interesting things about this sample is the blue shift of the exciton peak after exposing the sample to air. This sample has well-defined peaks and it was easy to define a value for the excitation peak. This blue shift is due to the oxidation because for the measurement under the microscope the samples have to be in air and not in a sample holder because otherwise it is impossible to find the right focus with the objectives. One way to protect the samples could be surface treatment.

3.1.2 Sample 2

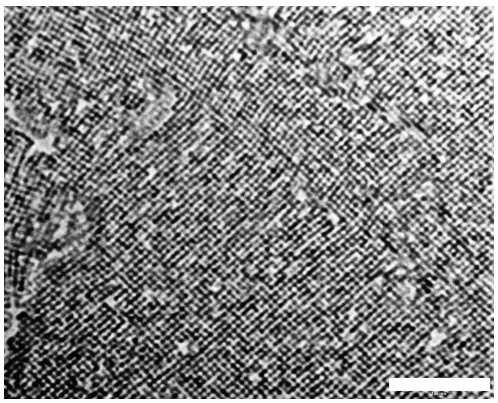

(a) 2A and 2B. Nice square structure with visible necking

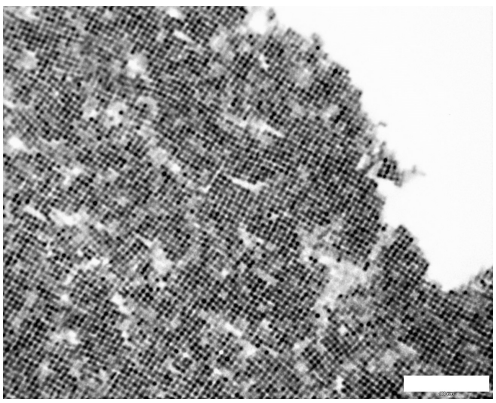

(b) 2C and 2D. The sample doesn't look completely homogeneous but at least there is a square structure visible

Figure 17: TEM samples of sample 2, scale bars 100 nm

Samples 2A and 2B are made via oriented attachment with a solution of 40 µL QDs, synthesised by the Owen Group, diluted in 2 mL toluene and 2C and 2D with a solution of 20 µL QDs, synthesised by Joep Peters MSc., diluted in 1 mL toluene. Both QDs are completely monodispersed and have the size of 5.7 nm. The FTIR data of sample 2 is presented in Fig. 18. The TEM picture of sample 2A and 2B shows nice long range square structure, however, the TEM image of sample 2C and 2D is less convincing because it is less homogeneous. Most of the FTIR absorption graphs of these samples have nice plateau shaped graphs and not so much the hill shaped structures, Fig. 18a. This says something about the 2D nature of the material as is described in Appendix A. It can be concluded that the connection between the particles is present and relatively strong and that the structures have a 2D nature. Important to note is that the different values of the exciton peak can come from the extended plateau of the graph. This plateau can be as large as approximately 200 nm and hence, it is not possible to conclude too much about shifts of the exciton peak.

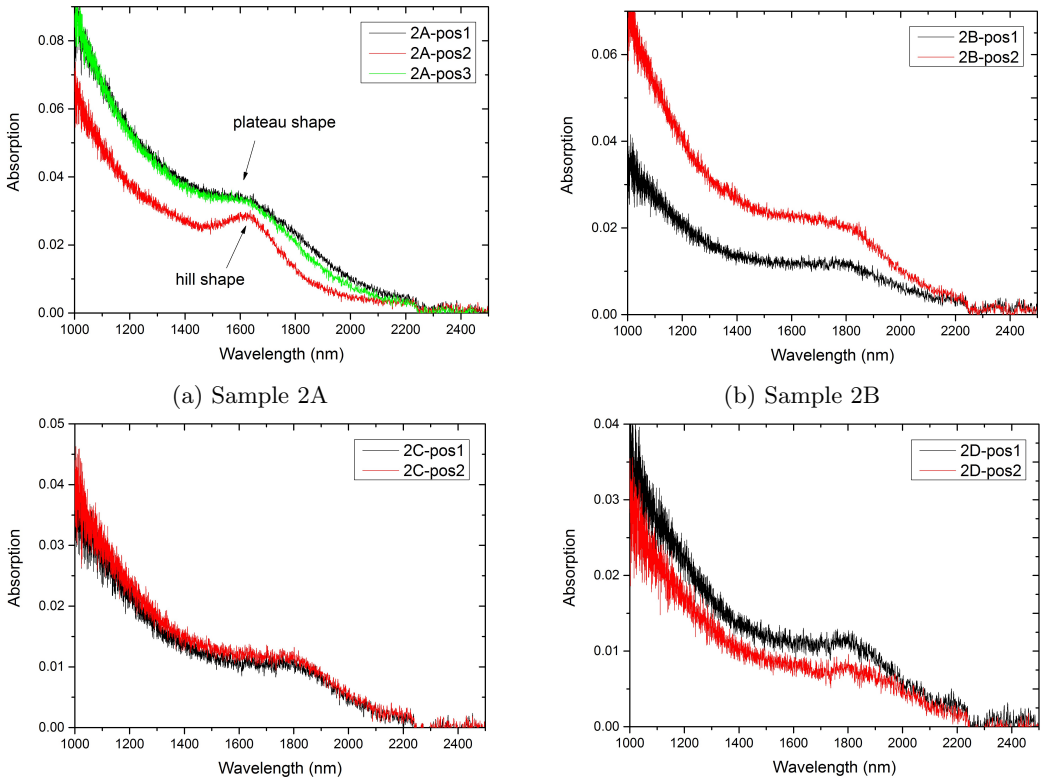

(a) Sample 2A

(b) Sample 2B

(c) Sample 2C

(d) Sample 2D

Figure 18: FTIR data

Sample	**Position**	**Absorption (%)**	**Wavelength (nm)**
2A	1	3.5	1565
	2	3.0	1620
	3	3.6	1565
2B	2	1.2	1782
	3	2.4	1650
2C	1	1.2	1700
	2	1.4	1700
2D	1	1.2	1797
	2	0.8	1790

Table 3: Absorption data of sample 2

However, this sample yields interesting information about the absorption. The samples again have values with a large deviation, Table 3. Let's first consider samples 2B, 2C and 2D. The difference might be caused by the inhomogeneity of the sample, as described previously in Sec. 3.1.1. When sample 2A is considered, the difference is quite large. The big difference is not very likely to come from the inhomogeneity of the sample. It could, however, come from a bilayer. It is possible that a double layer forms instead of a single layer. This would make much more sense, because the values would fit the other results by considering it to be a doubled absorption quantum.

3.1.3 Sample 3

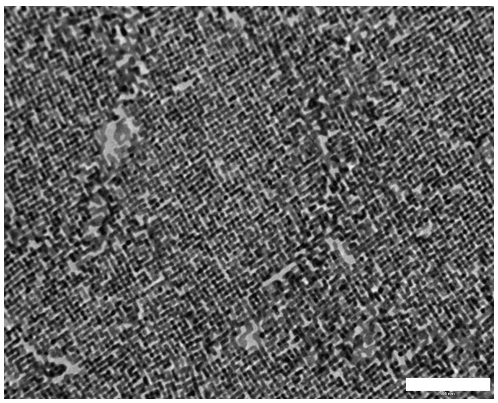

(a) 3A. Square structure is clearly visible, also in large regions of the sample, scale bar 100 nm

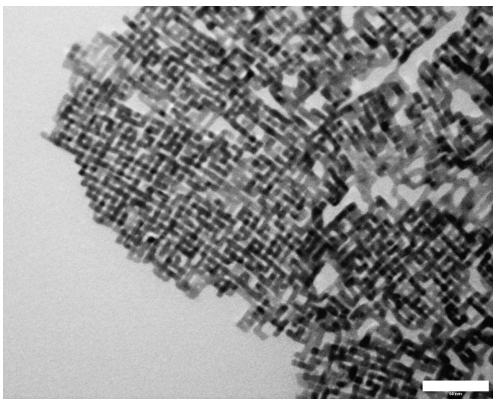

(b) 3B. The sample doesn't look completely homogeneous but at least there is a square structure, scale bar 50 nm

Figure 19: TEM pictures of sample 3

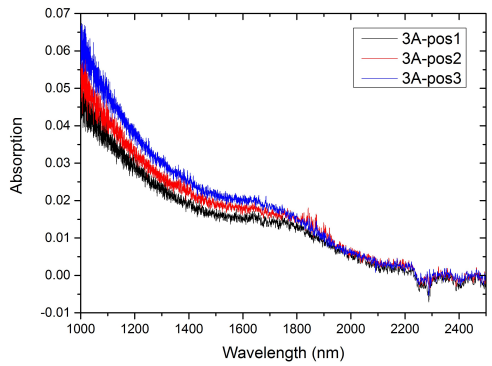

(a) Sample 3A

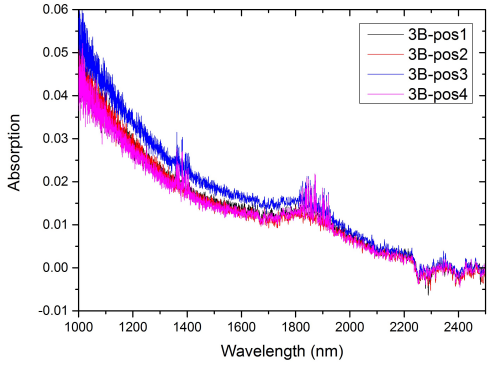

(b) Sample 3B

Figure 20: FTIR data

Sample	Position	Absorption (%)	Wavelength (nm)
3A	1	1.7	1642
	2	2.0	1642
	3	2.1	1642
3B	1	1.3	1842
	2	1.2	1815
	3	1.6	1834
	4	1.3	1804

Table 4: Absorption data of sample 3

Sample 3 is made via oriented attachment with a solution of 20 µL QDs diluted in 1 mL toluene. The FTIR data of sample 3 is presented in Fig. 20 and Table 4. From the TEM pictures, Fig. 19, it is possible to conclude that the samples have square structures. The TEM picture of 3A has a long range ordering, sample 3B is less convincing. The FTIR data of both sample 3A and 3B has plateau shaped graphs, but sample 3B has some extra noise. The noise might

be caused by the sample holder used for the FTIR analysis and it is still possible to derive a certain value from the graph. The big differences in absorption energy, Table 4 are caused by the plateau shaped peaks. The absorption data has again differences. This might be caused by inhomogeneity of the samples, as described previously.

When the values of all the samples are collected and the mean value and standard deviation is calculated a value of $1.5 \pm 0.4\%$ is obtained. This value has a large standard deviation, at least too large to draw immediate conclusions.

3.2 Fluorescence microscope

To illustrate the principle of the fluorescence microscopy to measure absorption and photo-luminescence of the superstructures and to demonstrate the performance of the set-up, some representative measurements of drop casted CdSe are showed.

3.2.1 Luminescence

The setup is perfectly designed for measuring luminescence in a sample, as described in the Experimental section2.3.3. Luminescence of a drop casted CdSe sample is measured, with a certain wavelength selected by the monochromator and with a laser light source of 441 nm. Both with laser light and with the tungsten-halogen light, luminescence is found, Fig. 21.

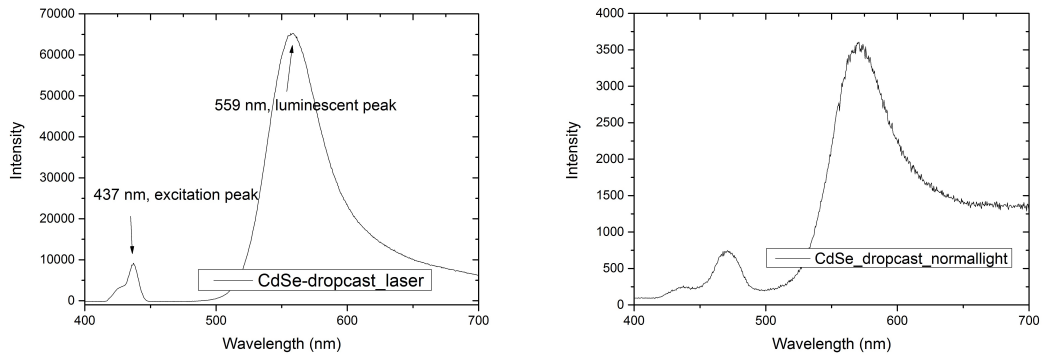

(a) Laser light source

(b) Normal light source

Figure 21: Luminescence experiment on drop casted CdSe sample

Still, the excitation peak is visible, both for the tungsten-halogen light (470 nm) source and the laser light source 437 nm. This is related to the dichroic beam splitter used in the setup. Despite the fact that this kind of beam splitters is designed to transmit and reflect in certain wavelength ranges, they don't work perfectly. The setup is not ready to carry out luminescence measurements in the Near InfraRed (NIR). A suitable beam splitter should be mounted and the objectives used are not designed for light in the NIR region.

3.2.2 Absorption

There are in general two ways of measuring absorption with the setup. The first method is to measure transmitted light from an empty quartz glass (as a background) and afterwards the quartz substrate with sample while exposing it to white light, i.e. the monochromator is not used. Then the amount of absorbed light by the sample can be calculated from the difference of those two transmission graphs. The other option is to make a sequence of data points by changing the value of the wavelength with the monochromator both for background and sample. For the latter, it would be really convenient to write an algorithm to measure

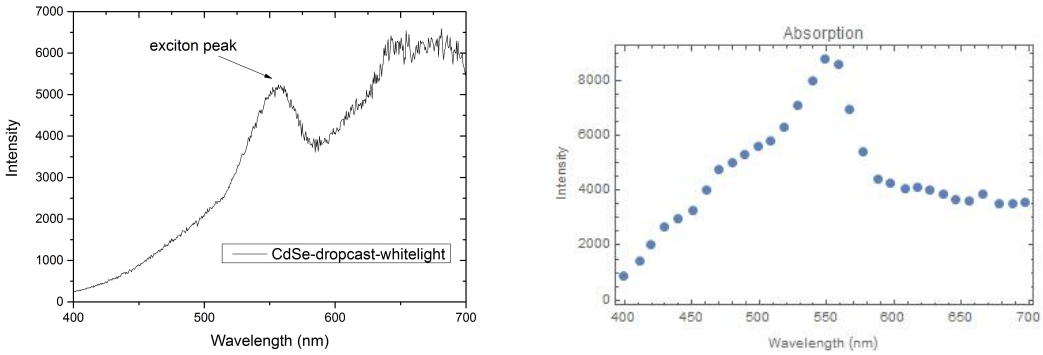

(a) Exposed to white light

(b) Sequence of single wavelengths

Figure 22: Absorption of a CdSe drop casted sample

in a fast way. However, it would be easier to use the former method, because it is faster, no algorithm is needed and the analysis is much faster.

As is visible in Fig. 22a the absorption peak is visible for a drop casted sample of CdSe QDs around 560 nm. However, because no monolayer sample is measured it is not sure if the resolution of the setup is good enough to measure a small value in the order of magnitude of 1%. Also, the usual absorption shape is not present, i.e. the value of the absorption should go up to higher energies (or lower wavelength).

The other method, with the sequence of different wavelengths, yielded results but it is not clear if those results are really the desired results, Fig.22b. A peak is found in the right spot, around 560 nm, but the normal absorption shape of quantum dots is not found. This might be a result of the low light intensity at lower wavelengths, but it is not sure whether that is the only reason or not. The two different methods yielded different absorption values, by a factor of 2. This might be caused by measuring a different spot of the sample, drop casted samples are usually not very homogeneous.

It is very important to avoid saturation of the detector. If the detector gets too much information to process, the region of interest is not analysed in the most optimal way. Saturation can easily be checked by taking half of the exposure time and check if the intensity is also half the value it had before for a certain wavelength. For the absorption measurements with the white light, a pinhole is placed between light source and collimating (convex) lenses to lower the light intensity on the detector.

4 Discussion and conclusions

4.1 Discussion

It is a promising result that a value in the right order of magnitude is found an that it is possible to measure absorption with FTIR spectroscopy, However, the large standard deviation still prevents the drawing of big conclusions. This can have several reasons which have to be discussed in this section. There are big differences in the different measurements. These differences should be overcome by making samples with a higher homogeneity or select good sample spots with the microscope. Then, the resolution should be better, otherwise the standard deviation of the measurement is higher compared to the differences of the samples. The main reason of the differences is still the inhomogeneity, if this can be overcome, the biggest issue is likely to be solved.

Still, the sample 2A has a high value. Dividing the value by two might seem a bit brute force. There are several reasons to do this. It is striking that the value is more or less exactly doubling the result from all other measurements. This points to the quantised character of the absorption of 2D systems. An extra layer would yield a doubled absorption. Also, compared to sample 2B, which should be the same, sample 2A is the double value. This points again to the double layer. Then the only problem is: how is it possible that a double layer has formed? The formation of a double layer is not impossible. It might be the oriented attachment procedure that produced the double layer locally or the concentration is accidentally doubled in the experiment.

The reflectivity of the sample is not considered, it's assumed to be zero. Reflectivity is measured with the FTIR under the microscope, but this method is not developed enough to yield any useful results. Reflectivity should be measured to really be sure about the absorption value.

According to sample 1, the blue shift due to oxidation is quite large. It might be a good step to do surface treatment on PbSe samples that are measured under the microscope in FTIR.

The fluorescence microscope works for drop casted samples, measured with the CCD-Vis camera in the visible region, both for absorption and luminescence measurements. As pointed out before, for absorption measurements it might be better to make use of the FTIR machine but it might be worth the try to fine-tune the method of the absorption measurement in the fluorescence microscope setup. For luminescence, the setup works in the visible region, but there are still two options concerning the light source. The laser light source shows promising results but there are two major drawbacks when working with this light source. At first, the monolayer might be melted by the highly intense laser beam. Secondly, the laser light source has only one wavelength to excite. It is, however, very convenient to change the wavelength of the tungsten-halogen light source with the monochromator. This might be an important feature to determine whether a certain peak is luminescent or not. A luminescence peak is believed to be always at the same energy and therefore not changing by changing the excitation energy. However, the intensity of the luminescent peak might change by altering the energy of the incident light. It is therefore more convenient to work with a tuneable light source. The laser as a light source is still an option but the tungsten halogen light source is considered the best option.

4.2 Conclusions

A value of $1.5 \pm 0.4\%$ is found for absorption of a 2D PbSe monolayer by FTIR measurements. This value is promising in order to find the absorption quantum of the 2D PbSe material but still has a too large standard deviation. It is not sure whether this is indeed a quantised value or not. More samples are needed to support an undoubtable conclusion.

The fluorescence microscope setup is well prepared to perform luminescence experiments in the visible region on 2D superstructures.

5 Outlook

It is necessary to have more samples of sufficient quality measured to really decrease the value of the standard deviation of the absorption and to determine the absorption quantum of PbSe 2D monolayers. It is convenient to have samples of good quality, with a high coverage of the substrate. This is to reduce the difference of the measurements as much as possible. Furthermore, the method with the microscope and the FTIR can be explored further. The method of the measurement is good enough but more experience has to be gained to work with the machine in a proper way. This microscope measurements could be really helpful, because the spot on the sample can really be chosen by the experimenter. However, the reflectivity of the 2D superstructures is not revealed yet. It is unknown if it influences the measurements in a significant way and therefore, more precise values will be obtained if the reflectivity can also be measured and considered. It is not sure yet if the absorption value is really quantised. This has to be checked by measuring more monolayers on top of each other.

The setup for luminescence works, in general. No monolayer samples are measured yet, but it is likely that those experiments can be carried out in the future. Especially the luminescence experiment would be really interesting, because luminescence yields a lot of information about the surface. Since 2D monolayers have a extraordinary high surface to volume ratio, information about surface quality would be really interesting. As described in the theory section 1.4, experiments at low T might yield really new information about the surface quality and energy transitions of the sample. The fluorescence microscope setup is suitable for low T experiments because the cryostat can be linked to a liquid helium vessel. This opens up a whole new range of possibly very interesting measurements. However, it is not sure whether the cation exchanged monolayers (Cd for Pb) have any luminescence. To counteract possibly quenched luminescence, samples can be treated for surface passivation. This would lower the surface defects and by chance enhance the luminescence.

6 Acknowledgements

Expressing thanks to people is the best part of writing a thesis. Daily supervisor Maryam Alimoradi Jazi, you are the real hero of this project. It was great fun to work with you! For those who wonder: Yes, research can be fun as well. The trip to Delft to collect samples and do experiments was the best example of this fun. Unfortunately, I got a lot of minus points for my witty remarks and by the time writing I cannot graduate anymore with the amount of minus's I have got. Let's hope for a lot of mercy. Also many thanks to Daniël Vanmaekelbergh who welcomed me, being a physicist, on his lab. Thanks a lot for the opportunity to work in this environment. Federico, Jaco, Ward, Matthijs and especially Joep for always being around and available for questions. Thank you, dear master students! Thanks for silently reminding me of my previous life as a chemist and that I am already studying for five years (great time!). Bachelor students, the time together was short, but nice! Lieven, thanks for helping out with LateX and Mendeley. Jesper, Mark and John BSc. (a.k.a. die Engelsman), thanks for playing numerous card games during lunch and coffee breaks.

A Density of states in multiple dimensions

In this section, an intuitive argument is developed for the existence of a plateau shaped instead of a hill shaped graph in the FTIR data for 2D systems via the density of states of an electron gas.

The density of states for both a zero-dimensional and a two-dimensional gas can easily be calculated[30]. The density of the 0D case can be represented by a delta-function because there is no free motion possible:

$$g(E)_{0D} \propto \delta(E). \tag{22}$$

The 2D case is somewhat more complicated because motion is possible in two directions. A derivation is done to show that the density of states is proportional to E^0, i.e. a constant.

At the start, we have the Schrödinger equation:

$$-\frac{\hbar^2}{2m}\nabla^2\Psi = E\Psi, \tag{23}$$

which is in two dimensions equal to:

$$\frac{d^2\Psi}{dx^2} + \frac{d^2\Psi}{dy^2} + k^2\Psi = 0, \tag{24}$$

with $k = \sqrt{2mE/\hbar^2}$.

When separation of variables is introduced, we have the following form of the wave function:

$$\Psi(x, y) = \Psi_x(x)\Psi_y(y). \tag{25}$$

Equation 24 can be written as:

$$\frac{1}{\Psi_x}\frac{d^2\Psi}{dx^2} + \frac{1}{\Psi_y}\frac{d^2\Psi}{dy^2} + k^2 = 0, \tag{26}$$

with k^2 a constant. Because k is a constant,

$$\frac{1}{\Psi_x}\frac{d^2\Psi}{dx^2} = \frac{1}{\Psi_y}\frac{d^2\Psi}{dy^2} = -k^2, \tag{27}$$

where $k^2 = k_x^2 + k_y^2$.

The solution of the wave function Ψ is, imposing boundary conditions of the wave function equalling zero at the infinite barriers of the potential well (our 2D system):

$$\Psi = A\sin(k_x x)\sin(k_y y), \tag{28}$$

with $k_{x,y} = n_{x,y}\pi/L$ where n is an integer. Now, the number of states in a 2D k-space is proportional to k^2:

$$N \propto k^2 \propto E \tag{29}$$

With N, it is possible to calculate the density of states:

$$\frac{dN}{dE} \propto E^0. \tag{30}$$

This implies that the density of states of a 2D electron gas is a step function, which can be represented with the Heaviside step function:

$$g(E)_{2D} \propto H(E). \tag{31}$$

Both the 0D and the 2D case can be visualised:

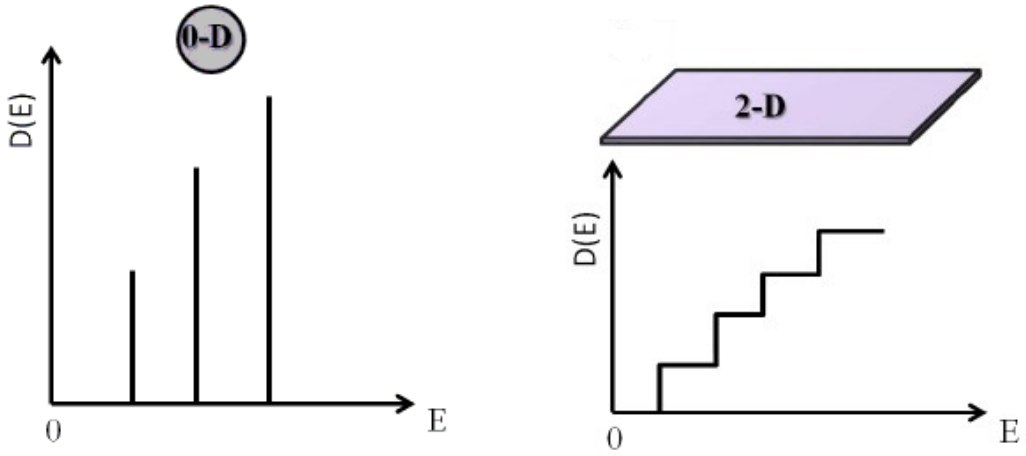

(a) 1D (b) 2D

Figure 23: Density of states [31]

Now, going from an electron gas to a system of quantum dots, that have a certain size distribution and therefore an exciton energy distribution caused by quantum confinement effects, the delta function broadens to a more realistic shape of the density of states. Intuitively, this corresponds to the system with the quantum dots in dispersion. For the 2D system, an analogous argument can be developed. The plateau shaped peaks are an indication that the system considered has more properties, at least the density of states, of a 2D system then properties of a 0D system. This can be recognised in the FTIR data presented in this thesis. The plateau shaped peaks are an indication of a 2D system and the hill shaped peaks point to a quantum dot.

References

[1] R. R. Nair, A. N. Grigorenko, P. Blake, K. S. Novoselov, T. J. Booth, N. M. R. Peres, T. Stauber, and A. K. Geim, "Fine Structure Constant Defines Visual Transparency of Graphene", *Science*, vol. 320, no. 5881, p. 1308, 2008, ISSN: 1095-9203. DOI: 10.1126/science.1156965. arXiv: 0803.3718v1. [Online]. Available: http://www.ncbi.nlm.nih.gov/pubmed/18388259.

[2] M. Reed, J. Randall, R. Aggarwal, R. Matyi, T. Moore, and A. Wetsel, "Observation of discrete electronic states in a zero-dimensional semiconductor nanostructure", *Physical review letters*, vol. 60, no. 6, pp. 535–537, Feb. 1988, ISSN: 0031-9007. DOI: 10.1103/PhysRevLett.60.535.

[3] C. de Mello Donegá, "Chapter 2. Size effects on Semiconductor Nanoparticles", in *Nanoparticles, workhorses of nanoscience*, 2014, p. 13.

[4] E. Kalesaki, C. Delerue, C. Morais Smith, W. Beugeling, G. Allan, and D. Vanmaekelbergh, "Dirac cones, topological edge states, and nontrivial flat bands in two-dimensional semiconductors with a honeycomb nanogeometry", *Physical review x*, vol. 4, no. 1, pp. 1–12, 2014, ISSN: 21603308. DOI: 10.1103/PhysRevX.4.011010. arXiv: arXiv:1502.04886v1.

[5] W. K. Bae, J. Joo, L. A. Padilha, J. Won, D. C. Lee, Q. Lin, W. K. Koh, H. Luo, V. I. Klimov, and J. M. Pietryga, "Highly effective surface passivation of pbse quantum dots through reaction with molecular chlorine", *Journal of the american chemical society*, vol. 134, no. 49, pp. 20 160–20 168, 2012, ISSN: 00027863. DOI: 10.1021/ja309783v.

[6] W. H. Evers, B. Goris, S. Bals, M. Casavola, J. De Graaf, R. V. Roij, M. Dijkstra, and D. Vanmaekelbergh, "Low-dimensional semiconductor superlattices formed by geometric control over nanocrystal attachment", *Nano letters*, vol. 13, no. 6, pp. 2317–2323, 2013, ISSN: 15306984. DOI: 10.1021/nl303322k. arXiv: 0706.1062v1.

[7] C. B. Farnsworth, *Color Will Come to Cool*, 2015. [Online]. Available: http://www.greenbuildermedia.com/news/blog/news/color-will-come-to-cool (visited on 05/27/2016).

[8] J. L. Peters, "Fabrication of single crystalline ultra-thin superlattices by self-assembly via oriented attachment of PbTe nanocrystals", 2013.

[9] S. van Rossum and C. van Overbeek, "Single crystalline PbS thin films via oriented attachment", 2014.

[10] Dongsheng Li, Michael H. Nielsen, Jonathan R. I. Lee Cathrine Frandsen and J. J. D. Y. Jillian F. Banfield, "Direction-Specific Interactions", *Science*, no. May, pp. 1014–1019, 2012.

[11] H. Zhang and J. F. Banfield, "Energy Calculations Predict Nanoparticle Attachment Orientations and Asymmetric Crystal Formation", *J. phys. chem. lett.*, vol. 3, no. 19, p. 2882, 2012, ISSN: 19487185. DOI: 10.1021/jz301161j.

[12] C. O'Mahony, R. Farell, J. D. Holmes, and M. A. Morris, "Chapter 13. The thermodynamics of defect formation in self-assembled systems", in *Thermodynamic systems in equilibrium and non-equilibrium*, 2011, p. 279.

[13] H. Fang, H. Bechtel, E. Plis, M. C. Martin, S. Krishna, E. Yablonovitch, and A. Javey, "Quantum of optical absorption in two-dimensional semiconductors", *Pnas*, vol. 110, no. 29, pp. 11 688–11 691, 2013.

[14] F. Rabouw, *Before there was light : Excited state dynamics in luminescent (nano)materials*. 2015, ISBN: 9789039363973. [Online]. Available: http://www.narcis.nl/publication/RecordID/oai:dspace.library.uu.nl:1874/328061.

[15] T. H. Gfroerer, "Photoluminescence in Analysis of Surfaces and Interfaces", *Encyclopedia of analytical chemistry*, pp. 9209–9231, 2000, ISSN: 0470027312. DOI: 10.1002/9780470027318.a2510. arXiv: 1404.6292.

[16] J. D. Puksec, "Recombination Processes and Holes and Electrons Lifetimes", *Issn*, vol. 43, pp. 47–53, 2002.

[17] H. Liu and P. Guyot-Sionnest, "Photoluminescence lifetime of lead selenide colloidal quantum dots", *Journal of physical chemistry c*, vol. 114, no. 35, pp. 14 860–14 863, 2010, ISSN: 19327447. DOI: 10.1021/jp105818e.

[18] S. T. Et al., "Defects activate photoluminescence in two-dimensional semiconductors: interplay between bound, charged and free excitons", *Sci. rep.*, vol. 3, no. 2657, 2013.

[19] P. Sippel, W. Albrecht, D. Mitoraj, R. Eichberger, T. Hannappel, and D. Vanmaekelbergh, "Two-photon photoemission study of competing auger and surface-mediated relaxation of hot electrons in CdSe quantum dot solids", *Nano letters*, vol. 13, no. 4, pp. 1655–1661, 2013, ISSN: 15306984. DOI: 10.1021/nl400113t.

[20] T. B. Hoang, L. V. Titova, H. E. Jackson, L. M. Smith, J. M. Yarrison-Rice, J. L. Lensch, and L. J. Lauhon, "Temperature dependent photoluminescence of single CdS nanowires", *Applied physics letters*, vol. 89, no. 12, pp. 1–11, 2006, ISSN: 00036951. DOI: 10.1063/1.2357003. arXiv: 0606428 [cond-mat].

[21] *TEM TRANSMISSION ELECTRON MICROSCOPE*. [Online]. Available: http://binoculas.net/tem-transmission-electron-microscope/ (visited on 06/10/2016).

[22] *Introduction to Fourier Transform Infrared Spectrometry*. [Online]. Available: http://mmrc.caltech.edu/FTIR/FTIRintro.pdf (visited on 06/13/2016).

[23] R. Blanchard, S. V. Boriskina, P. Genevet, M. A. Kats, J.-P. Tetienne, N. Yu, M. O. Scully, L. D. Negro, and F. Capasso, *Multi-wavelength mid-infrared plasmonic antennas with single nanoscale focal point*. [Online]. Available: https://www.osapublishing.org/oe/fulltext.cfm?uri=oe-19-22-22113%7B%5C&%7Did=223790 (visited on 06/08/2016).

[24] *Optical Characterization of Inorganic Semiconductors*. [Online]. Available: http://www.slideshare.net/RobertTreharne/optical-characterization-of-inorganic-semiconductors (visited on 06/08/2016).

[25] *What Is A CCD?* [Online]. Available: http://www.specinst.com/What%7B%5C_%7DIs%7B%5C_%7DA%7B%5C_%7DCCD.html (visited on 05/12/2016).

[26] A. Meijerink, *Nanophotonics, Lecture Notes NCCN-course, Lecture 3, Light Detectors and Monochromators*, Sep. 2015.

[27] *CCD description and characteristics*. [Online]. Available: http://www.astro.ugto.mx/cursos/Laboratorio/CCD%7B%5C&%7DReduccion%7B%5C_%7Dp1.pdf (visited on 05/12/2016).

[28] Thorlabs, *Longpass Dichroic Mirrors/Beamsplitters*. [Online]. Available: http://www.thorlabs.de/newgrouppage9.cfm?objectgroup%7B%5C_%7Did=3313 (visited on 06/13/2016).

[29] *Refractive index database*. [Online]. Available: http://refractiveindex.info/?shelf=main%7B%5C&%7Dbook=SiO2%7B%5C&%7Dpage=Malitson (visited on 06/07/2016).

[30] *Density of States: 2D, 1D, and 0D*. [Online]. Available: http://users.ece.gatech.edu/%7B~%7Dalan/ECE6451/Lectures/StudentLectures/King%7B%5C_%7DNotes%7B%5C_%7DDensity%7B%5C_%7Dof%7B%5C_%7DStates%7B%5C_%7D2D1D0D.pdf (visited on 06/11/2016).

[31] *White LEDs Printed on Paper A Doctoral Thesis Part I*. [Online]. Available: http://www.edn.com/Home/PrintView?contentItemId=4391796 (visited on 06/11/2016).